Computers and Fluids 159 (2017) 232–242

Contents lists available at ScienceDirect

Computers and Fluids

journal homepage: www.elsevier.com/locate/compfluid

Thermal lattice Boltzmann study of three-dimensional bubble growth in quiescent liquid

Xiangting Chang, Haibo Huang*, Xi-Yun Lu

Department of Modern Mechanics, University of Science and Technology of China, Hefei, Anhui 230026, China

ARTICLE INFO

Article history:
Received 15 May 2017
Revised 22 August 2017
Accepted 3 October 2017
Available online 4 October 2017

Keywords:
Lattice Boltzmann method
Multiphase
Thermal
Boundary condition
Level-set
Bubble growth

ABSTRACT

The complete growth process of a single bubble in quiescent liquid is simulated using a three-dimensional hybrid thermal lattice Boltzmann model. The non-equilibrium extrapolation pressure boundary condition is extended to handle the thermal multiphase flow. Unfavorable spurious currents are usually generated in the vicinity of curved interfaces when two-phase lattice Boltzmann methods are applied. Here a level-set scheme is incorporated into the simulations to accurately represent interfacial dynamics. The phase change is controlled by an equation of state automatically instead of any artificial phase change model. Hence the present simulation is more accurate and thermodynamically consistent. The temperature, velocity fields during the bubble growth are consistent with relevant theories. The bubble growth rate obtained from the lattice Boltzmann simulations agree well with the analytical solutions. The result shows that the present scheme is able to simulate the relevant thermal bubble dynamics quantitatively.

1. Introduction

Boiling heat transfer is a heat transfer mode during the phase change of liquid to vapor. Because of its high heat transfer efficiency and extensive industrial applications, a lot of studies have been carried out to explore the mechanism of boiling heat transfer. Bubble growth plays a key role in the boiling. Usually the growth procedure can be divided into two stages: isothermal stage and isobaric stage [1]. A large amount of experimental work [2,3] was implemented to study the bubble growth, and some theoretical formulas were also obtained through experiments [4–6]. However, due to the limitations of experimental study, the mechanism and heat transfer characteristics during bubble growth are not well understood. Over the past decade, with the rapid development of computer technology and numerical methods, Computational Fluid Dynamics (CFD) has become an effective tool for studying bubble growth and boiling problem.

Nucleate boiling has been investigated numerically using the level-set method [7] and the volume of fluid (VOF) method [8]. Two-dimensional (2D) simulation of nucleate boiling was also carried out using the VOSET method [9], which combines the advantages of VOF and level-set methods. A mesh-free method is also applied to study bubble departure from the heated surface [10]. However, the methods mentioned above have to track or reconstruct the vapor-liquid interfaces. To track the interfaces, special treatments are necessary [11], in which artificial corrections may have to be incorporated. That may decrease the numerical accuracy.

The lattice Boltzmann method (LBM) has been widely used in simulating multiphase flows in recent years. It is based on mesoscopic kinetic equations. Comparing with conventional methods for multiphase flows, LBM does not track interfaces explicitly while sharp interfaces can be maintained. LBM has also been successfully applied to study wetting and spreading phenomena [12,13], bubble collision and bubble rising phenomena [14–16], etc.

There are several popular multiphase lattice Boltzmann (LB) models in the literature. The first type is the color-gradient model proposed by Gunstensen et al. [17] which is developed from the Rothman–Keller lattice gas model [18]. The second type is the Shan–Chen (SC) model [19], which is a pseudopotential model. The third type is free-energy-based model [20]. The last one is proposed by He et al. [21] which uses the idea of phase field. Among them the Shan–Chen pseudopotential lattice Boltzmann model has become the most popular one.

In the multiphase LBM, phase change model is also important. For phase change models, there are two popular ones in the LBM literature. One is the two-phase LB model with an artificial evaporation model. The other is the thermodynamic consistent two-phase LBM with equation of state (EOS). The former one has no explicit EOS and evaporation model comes from phenomenology study (Stefan problem) [22,23]. For example, in Ref. [22], the droplet evaporation was simulated using the two-phase LBM based

* Corresponding author.
E-mail address: huanghb@ustc.edu.cn (H. Huang).

https://doi.org/10.1016/j.compfluid.2017.10.005
0045-7930/

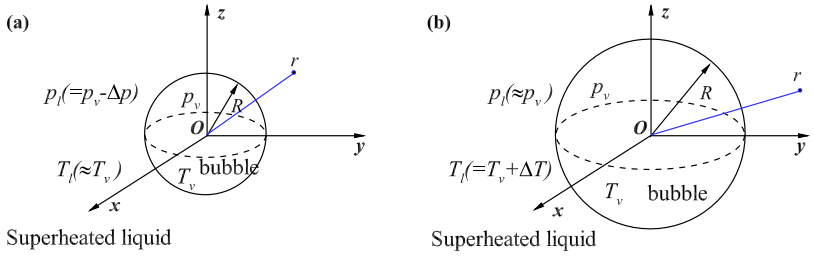

Fig. 1. The schematic diagram for the bubble growth stage. (a) the isothermal growth and (b) the isobaric growth. *p, T* represent pressure and temperature, respectively. The subscripts '*l*', '*v*' denote liquid and vapor, respectively. Δp and ΔT are an additional pressure and superheat, respectively. *R* is the bubble radius and *r* is a distance between a point in the liquid and the bubble center. The origin of coordinates (0,0,0) is located at the center of the computational domain.

on Ref. [24]. In the scheme, the gradient of the vapor concentration at the liquid-vapor interface is included as the driving force for vaporization. For the latter one, the temperature field is governed by the energy equation and the temperature in the flow field is coupled with that in the equation of state. The energy equation can be solved by a LB scheme [11] or the Runge–Kutta scheme [25].

The Shan–Chen model with different EOS has been further developed to simulate thermal two-phase flows [11,25–30]. Using the thermal Shan–Chen LBM, quantitative analyses for the bubble departure from a horizontal plate in heterogeneous boiling were carried out [11,26]. Gong and Cheng also applied the model to study the bubble nucleation, growth, and departure in presence of a heated wall [28,29]. Biferale et al. [27] applied the three-dimensional (3D) thermal Shan–Chen model for simulating the convection in multiphase flows. Li et al. [25] used the scheme to study the film boiling process. Fang et al. [30] adopted a MRT pseudopotential thermal LBM to simulate the pool boiling. In the above LBM studies, bubble departure and rising are focused. However, the bubble growth process has not been studied systematically using the LBM.

For the bubble growth in the superheated quiescent liquid, the first stage is isothermal growth stage [1]. In this stage, the bubble is very small and the pressure inside the bubble is larger than that outside. Bubble gradually increases due to the inertial force, the viscous force, and the surface tension. During this process, the temperature inside and outside the bubble are approximately identical, the effect of heat transfer can be neglected. The schematic diagram for the isothermal growth is shown in Fig. 1(a). As the bubble grows, the internal pressure of the bubble decreases till it reaches the pressure of the quiescent liquid. The temperature inside the bubble also decreases and it becomes lower than that outside. At this point, the bubble growth enters the second stage: the isobaric stage. Its schematic diagram is shown in Fig. 1(b). The heat transfer of the superheated liquid around the bubble plays a key role in this stage.

For the droplet evaporation, some LBM studies have been carried out [22,31,32]. For bubble growth, the LBM studies are seldom. For example, the Shan–Chen multiphase flow model has been used to study the isothermal growth stage for a bubble [33], in which the temperature was constant and the heat transfer was not considered. In their study, the isobaric growth stage was not investigated. Besides, in the work of Chen et al. [33], the bubble is 2D, which is very different from the 3D cases because the isothermal bubble growth rates for 2D and 3D are different (see Appendix A derivation). Ryu and Ko [23] applied a free-energy-based LBM [34] to simulated the complete bubble growth process. In the study, an artificial phase change model [35] is used and there is no EOS. Without the EOS, the simulation may be not thermodynamically consistent. Moreover, the comparison between their LBM results and the analytical solutions is not so good.

In this paper, the two bubble growth processes including isothermal and isobaric stages, were studied completely using a three-dimensional hybrid thermal Shan–Chen LBM. In the method, the energy equation is solved by the second-order Runge–Kutta method. Because the EOS is used, the phase transition is automatic and thermodynamically consistent. An improved non-equilibrium extrapolation pressure boundary condition is developed for the superheated boundary. A level-set scheme is incorporated into the simulations to correct the spurious currents in the vicinity of the curved interface. In the following Section 2, the LBM is introduced briefly. The pressure boundary condition for superheated liquid and correction of the spurious currents are also elucidated. The LBM is validated in Section 3. The LBM results for bubble growth at the isothermal and isobaric stage are discussed in Section 4.

2. Numerical method

2.1. Shan–Chen single-component two-phase LBM

Here we implement the SC LBM [19] in three dimensions for a single-component two-phase system. In the model, one distribution function is introduced for the fluid. The distribution function satisfies the following lattice Boltzmann equation:

$$f_a(\mathbf{x}+\mathbf{e}_a\Delta t, t+\Delta t) = f_a(\mathbf{x},t) - \frac{\Delta t}{\tau}\left(f_a(\mathbf{x},t) - f_a^{eq}(\mathbf{x},t)\right), \qquad (1)$$

where $f_a(\mathbf{x}, t)$ is the density distribution function in the ath velocity direction and τ is a relaxation time which is related to the kinematic viscosity as $\nu = c_s^2(\tau - 0.5\Delta t)$, where c_s is the lattice sound speed. The equilibrium distribution function $f_a^{eq}(\mathbf{x}, t)$ can be calculated as

$$f_a^{eq}(\mathbf{x},t) = w_a\rho\left[1 + \frac{\mathbf{e}_a\cdot\mathbf{u}^{eq}}{c_s^2} + \frac{(\mathbf{e}_a\cdot\mathbf{u}^{eq})^2}{2c_s^4} - \frac{(\mathbf{u}^{eq})^2}{2c_s^2}\right]. \qquad (2)$$

In Eqs. (1) and (2), the $\mathbf{e}_a$'s are the discrete velocities. For the D3Q19 model, they are given by

$$[\mathbf{e}_0,\mathbf{e}_1,\mathbf{e}_2,\mathbf{e}_3,\mathbf{e}_4,\mathbf{e}_5,\mathbf{e}_6,\mathbf{e}_7,\mathbf{e}_8,\mathbf{e}_9,\mathbf{e}_{10},\mathbf{e}_{11},\mathbf{e}_{12},\mathbf{e}_{13},\mathbf{e}_{14},\mathbf{e}_{15},\mathbf{e}_{16},\mathbf{e}_{17},\mathbf{e}_{18}]$$
$$= c\begin{bmatrix} 0 & 1 & -1 & 0 & 0 & 0 & 0 & 1 & -1 & 1 & -1 & 1 & -1 & 1 & -1 & 0 & 0 & 0 & 0 \\ 0 & 0 & 0 & 1 & -1 & 0 & 0 & 1 & 1 & -1 & -1 & 0 & 0 & 0 & 0 & 1 & -1 & 1 & -1 \\ 0 & 0 & 0 & 0 & 0 & 1 & -1 & 0 & 0 & 0 & 0 & 1 & 1 & -1 & -1 & 1 & 1 & -1 & -1 \end{bmatrix}.$$

In Eq. (2), for the D3Q19 model, w_a= 1/3 (a= 0), w_a= 1/18, (a= 1,...6), w_a =1/36, (a= 7,...18), $c_s = \frac{c}{\sqrt{3}}$, where $c = \frac{\Delta x}{\Delta t}$ is the ratio of lattice spacing Δx and time step Δt. Here, we define 1 lattice unit (Δx) as 1 *lu* and 1 time step (Δt) as 1 *ts*. '*mu*' denotes the mass

unit. In Eq. (2), ρ is the density of the fluid, which can be obtained from $\rho = \sum_a f_a$.

In the SC LBM, the effect of body force is incorporated through adding an acceleration into velocity field. The macroscopic velocity $\mathbf{u}^{eq}$ is given by

$$\mathbf{u}^{eq} = \mathbf{u}' + \frac{\tau \mathbf{F}}{\rho}, \tag{3}$$

where $\mathbf{u}'$ is the velocity defined as

$$\mathbf{u}' = \frac{\sum_a f_a \mathbf{e}_a}{\rho}. \tag{4}$$

In Eq. (3), $\mathbf{F} = \mathbf{F}_{int}$ is the inter-particle force. The actual whole fluid velocity $\mathbf{u}$ is defined as [12]:

$$\mathbf{u} = \mathbf{u}' + \frac{\mathbf{F}}{2\rho}, \tag{5}$$

which means the "fluid velocity" should be calculated correctly by averaging the momentum before and after the collision [12]. The inter-particle force is defined as [36],

$$\mathbf{F}_{int}(\mathbf{x}, t) = -G\psi(\mathbf{x}, t) \sum_a w_a \psi(\mathbf{x} + \mathbf{e}_a \Delta t, t)\mathbf{e}_a, \tag{6}$$

where G is a parameter that controls the strength of the inter-particle force and ψ is a effective number density [19]. Originally, Shan and Chen [19] proposed that,

$$\psi(\rho) = \rho_0[1 - \exp(-\rho/\rho_0)], \tag{7}$$

where ρ_0 is a constant.

Through Taylor expanding as described in the Appendix A in Ref. [37] and $-\partial_j p + \partial_i\left(c_s^2 \rho\right) = F_i$, here i, j means the x or y coordinates, we obtained the pressure p as [37]:

$$p = c_s^2 \rho + \frac{c_s^2 G}{2}\psi^2. \tag{8}$$

According to the Yuan and Schaefer [38], if the EOS of $p = p(\rho, T)$ is already known, we can use the following formula

$$\psi = \sqrt{\frac{2(p - c_s^2\rho)}{c_s^2 G}} \tag{9}$$

to incorporate different EOS into the SC LBM. Actually if Eq. (9) is adopted, G is only an auxiliary parameter, which is required to ensure that the whole term inside the square root is positive [38].

Here we use the van der Waals EOS which is the most classic EOS for non-ideal gas. It is given by

$$p = \frac{\rho RT}{1 - b\rho} - a\rho^2, \tag{10}$$

where R is the ideal gas constant. The critical properties for the EOS, such as p_c, T_c can be obtained by performing the first and second derivatives of pressure with respect to density to be zero. Then a and b can be presented as functions of p_c and T_c, i.e., $a = 27(RT_c)^2/64p_c$ and $b = RT_c/8p_c$. Following Refs. [20,38], the parameters are chosen as $R = 1$, $a = 9/49$, and $b = 2/21$.

2.2. Energy equation

Two schemes are commonly used to solve the energy equation in the thermal LBM: double-distribution-function (DDF) scheme [26] and finite-difference scheme. Neglecting the viscous heat dissipation, the energy equation can be written as [25]

$$\rho c_v \frac{DT}{Dt} = \nabla \cdot (\kappa \nabla T) - T\left(\frac{\partial p}{\partial T}\right)_\rho \nabla \cdot \mathbf{u}, \tag{11}$$

where κ is the thermal conductivity and c_v is the specific heat at constant volume.

If another lattice Boltzmann evolution equation is used to solve the energy equation [26], the scheme may introduce a spurious term into the macroscopic energy equation [25]. So here the finite-difference scheme is directly used to solve Eq. (11). To apply finite-difference scheme, Eq. (11) can be rewritten as

$$\partial_t T = -\mathbf{u} \cdot \nabla T + \frac{1}{\rho c_v}\nabla \cdot (\kappa \nabla T) - \frac{T}{\rho c_v}\left(\frac{\partial p}{\partial T}\right)_\rho \nabla \cdot \mathbf{u} \equiv M(T). \tag{12}$$

To solve Eq. (12), here the second-order Runge–Kutta method is used,

$$T(\mathbf{x}, t + \Delta t) = T(\mathbf{x}, t) + \frac{\Delta t}{2}(h_1 + h_2), \tag{13}$$

where h_1 and h_2 represent

$$h_1 = M[T(\mathbf{x}, t)], \qquad h_2 = M\left[T(\mathbf{x}, t) + \frac{\Delta t}{2}h_1\right]. \tag{14}$$

For the first derivative in Eq. (12), the second-order central discretization is adopted as follows

$$\frac{\partial \phi}{\partial x_i} = \sum_{a \neq 0} \frac{w_a \mathbf{e}_a \cdot \mathbf{i}[\phi(\mathbf{x} + \mathbf{e}_a \Delta t) - \phi(\mathbf{x} - \mathbf{e}_a \Delta t)]}{2c_s^2 \Delta t}, \tag{15}$$

where ϕ denotes a physical variable, $\mathbf{i}$ is the unit vector pointing along the i-coordinate axis. For the van der Waals EOS (Eq. (10)), $\left(\frac{\partial p}{\partial T}\right)_\rho = \frac{\rho R}{1 - b\rho}$, it is a function of ρ. It can be calculated directly from ρ. The second order derivative terms can be calculated by applying the first order derivative in Eq. (15) twice.

2.3. Correction of the spurious currents

Spurious currents are usually generated in the vicinity of curved interfaces when the Shan–Chen LBM is applied. Spurious velocities are not preferred and it may confound the accurate representation of interfacial dynamics [39]. There are some techniques can be adopted to eliminate the spurious currents, e.g., extending the spatial range of the pseudopotential interaction [40]. Recently, a simple level-set scheme is incorporated into the simulations to handle the problem [39]. Using the scheme, the interface velocity can be determined accurately even when spurious currents are generated [39].

The level-set equation is [39]

$$\frac{\partial \rho}{\partial t} + \zeta |\nabla \rho| = 0, \tag{16}$$

where ζ denotes the interfacial velocity magnitude in the direction normal to the interface. ζ can be calculated from rearranging the level-set equation, i.e., [39]

$$\zeta = -\frac{\partial \rho}{\partial t}/|\nabla \rho|. \tag{17}$$

It is noted that the normal vector to the lower-density phase can be computed as the gradient of the phase density field evaluated on by $\mathbf{n} = \frac{\nabla \rho}{|\nabla \rho|}$.

In the vicinity of curved interfaces, the level-set scheme [39] modifies actual fluid velocity $\mathbf{u}$ in Eq. (6) instead of $\mathbf{u}^{eq}$, i.e., the modified velocity is $\mathbf{u} = \zeta \mathbf{n}$. The time derivative $\frac{\partial \rho}{\partial t}$ at each node is calculated from the simple temporal difference $\frac{\partial \rho}{\partial t} = \frac{\rho^t - \rho^{t-\Delta t}}{\Delta t}$.

It is seen that actually in the above level-set scheme [39], the modified velocities are obtained through the change of interface locations at two continuous time steps. In the implementation, the gradient of density $\nabla \rho$ at each node can be calculated. The largest density gradient $(\nabla \rho)_{\max}$ in the flow field can be obtained,

which should appear in the vicinity of the interface in our simulations. Then, we only modify the velocities in the points with $\nabla\rho < \frac{1}{2}(\nabla\rho)_{\max}$, which confined the modified velocities only in the vicinity of the interface. The coefficient $\frac{1}{2}$ is obtained by trial and error in our simulations, which may be changed in other two-phase flow problems.

2.4. Pressure boundary condition for superheated liquid

For single phase flow, pressure boundary condition can be implemented through the non-equilibrium extrapolation scheme [41]. In the scheme, the distribution function on the boundary node is supposed to be composed of the equilibrium and non-equilibrium parts. The non-equilibrium part is extrapolated from that of the nearest interior fluid node and the equilibrium part is calculated by Eq. (2). When the equilibrium part is calculated, the density and velocity are required. If density is specified, the velocity should also be extrapolated from the nearest interior fluid node [41].

For single phase flow, in the LBM the pressure is a linear function of the density. The pressure boundary condition is implemented through specifying the density in the boundary. However, for two-phase flow, due to the van der Waals EOS, the pressure is a function of both temperature and density, which is different from that in the single phase flow.

To simulate the bubble growth, constant pressure boundary condition with a superheat should be imposed in the following way. Suppose at beginning, the temperature of the liquid is T_0, the corresponding saturated vapor pressure and the liquid density are p_0 and ρ_{l0}, respectively. The p_0, T_0 and ρ_{l0} should conform Eq. (10). Then the Dirichlet thermal boundary condition $T = T_0 + \Delta T$ with a superheat of ΔT is specified at boundary nodes. On the other hand, to ensure the constant pressure p_0 at boundary, the density on the boundary has to be reduced by $\Delta\rho$ when calculating the equilibrium distribution function, i.e., the density on the boundary is specified as $\rho_l = \rho_{l0} - \Delta\rho$. It is noted that $p = p_0$, $T = T_0 + \Delta T$, and $\rho_l = \rho_{l0} - \Delta\rho$ satisfies Eq. (10), i.e.,

$$p_0 = \frac{(\rho_{l0} - \Delta\rho)R(T_0 + \Delta T)}{1 - b(\rho_{l0} - \Delta\rho)} - a(\rho_{l0} - \Delta\rho)^2, \tag{18}$$

and then $\Delta\rho$ can be obtained. In this way, at the boundary, pressure is constant and superheat ΔT is also imposed. In the Shan–Chen model, when the equilibrium part is calculated, the density, velocity, and inter-particle force are required (see Eqs. (2) and (3)). If density is specified, the velocity and inter-particle force should also be extrapolated from the nearest interior fluid node.

3. Coexistence curve of the EOS, surface tension, and latent heat

In this section, coexistence curve obtained from the LBM simulations was compared to the analytical one. The analytical coexistence curve obtained from the Maxwell construction [42] is shown in Fig. 2(a). To check whether the equilibrium coexistence densities of the liquid and the vapor are consistent with the analytical ones, test cases of a droplet immersed in vapor in the absence of gravity are simulated. In our simulations, the computational domain is $100 \times 100 \times 1$ and periodic boundary conditions are applied on all boundaries. A circular area in the center of the domain is initialized as liquid area (higher density ρ_{li}) while the other region is initialized with vapor (ρ_{vi}) at lower density. ρ_{li} and ρ_{vi} are chosen to be close to the analytical liquid and vapor densities, respectively.

After the simulations reach the equilibrium state, we check the equilibrium densities of the liquid and vapor. For each case at different temperature, $\tau = 0.6$ and $\tau = 1.0$ were performed. The convergence criterion can be set based on the radius of the droplet or the spurious currents reaching a constant value, for example, $E_{\mathbf{u}} < 0.5\%$ over 1000 ts, where

$$E_{\mathbf{u}} = \sqrt{\frac{\sum_{\mathbf{x}}(|\mathbf{u}(\mathbf{x},t) - \mathbf{u}(\mathbf{x},t-1000\Delta t)|^2)}{\sum(|\mathbf{u}(\mathbf{x},t)|^2)}}. \tag{19}$$

It is noted that there is no velocity corrrection in these simulations. For a typical simulation with $\frac{T}{T_c} = 0.85$ and $\tau = 0.6$, initially the density inside a circular droplet with a radius of $R_i = 30\,lu$ is set to be $\rho_{li} = 6.3\,mu/lu^3$ and the other area is set to $\rho_{vi} = 1.3\,mu/lu^3$. At the equilibrium state, the densities are $\rho_v = 1.179\,mu/lu^3$, $\rho_l = 6.331\,mu/lu^3$. Radius of the droplet may change a little bit but the whole mass is conserved.

Through simulating many cases at different T, and measuring the densities, we can recover the coexistence curve. Fig. 2(a) shows the LBM results for $T/T_c = 0.8$, 0.825, 0.85, ...compared with the analytical coexisting densities. It demonstrates that the LBM results for $\tau = 0.6$ and $\tau = 1.0$ are all consistent with the analytical one except small discrepancies for the density of vapor.

The surface tension σ can be calculated numerically using the Laplace's formula. For two-dimension cases, the Laplace's law can be expressed as $\Delta p = \frac{\sigma}{R}$. In the above typical simulation, the equilibrium pressures inside and outside of the bubble are $p_{in} = 0.38986\,mu/(lu\,ts^2)$ and $p_{out} = 0.38259\,mu/(lu\,ts^2)$, respectively and the pressure difference $\Delta p = p_{in} - p_{out} = 0.00727\,mu/(lu\,ts^2)$. The radius of the droplet is $R = 29.22\,lu$. It is noted that the interface is supposed to be located at $\rho_s = \frac{(\rho_l+\rho_v)}{2}$. Hence the surface tension is $\sigma = \Delta pR = 0.212\,mu/ts^2$. More accurate σ can be obtained through linear fit in $\Delta p - \frac{1}{R}$ plot where results of several cases with different initial bubble sizes are presented [42]. From Fig. 2(b), it is seen that the surface tensions at different T calculated from the LBM are consistent with the analytical solutions.

The specific latent heat λ would be used extensively in the following study. Fig. 3 shows the latent heat as a function of temperature. λ can be calculated from the enthalpy of liquid and vapor, i.e.,

$$\lambda = h_v - h_l, \tag{20}$$

where v and l denote the vapor and liquid phases, respectively. For van der Waals gas, the internal energy can be written as

$$u = c_v T - a\rho. \tag{21}$$

Using the definition of enthalpy $h = u + pv$, we have

$$h = c_v T - a\rho + \frac{p}{\rho}. \tag{22}$$

Finally the latent heat for van der Waals EOS (Eq. (10)) can be calculated from

$$\begin{aligned}\lambda &= h_v - h_l = \left[-a\rho + \frac{p}{\rho}\right]_v - \left[-a\rho + \frac{p}{\rho}\right]_l \\ &= -2a(\rho_v - \rho_l) + RT\left(\frac{1}{1-b\rho_v} - \frac{1}{1-b\rho_l}\right).\end{aligned} \tag{23}$$

Substituting the densities of the liquid and vapor at temperature T, we have the latent value at T. The result is shown in Fig. 3.

4. Results and discussions

4.1. Isothermal growth stage

Isothermal growth stage is the initial stage during bubble growth. At beginning, the bubble is small and the pressure inside the bubble is very high. In this stage, the growth of the bubble is mainly dominated by the inertial force. It is an inertia-controlled stage, in which the effect of heat transfer can be neglected.

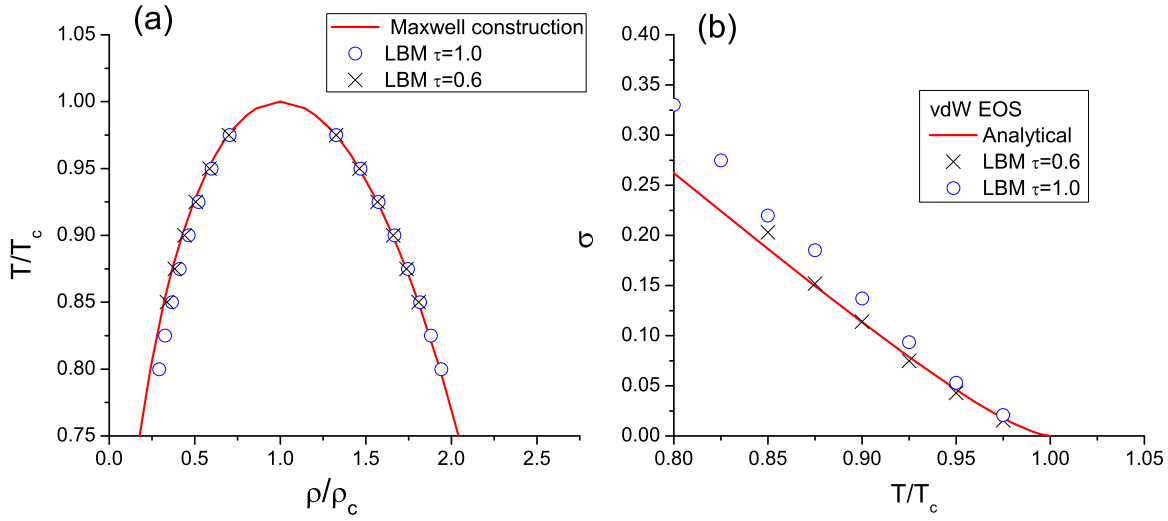

Fig. 2. (a) Coexistence curve of the van der Waals fluid. In the EOS (i.e., Eq. (10)), $a = \frac{9}{49}$, $b = \frac{2}{21}$, and $R = 1$. The corresponding critical density and temperature are $\rho_c = \frac{7}{2}$ and $T_c = \frac{4}{7}$, respectively. (b) the surface tension as a function of $\frac{T}{T_c}$.

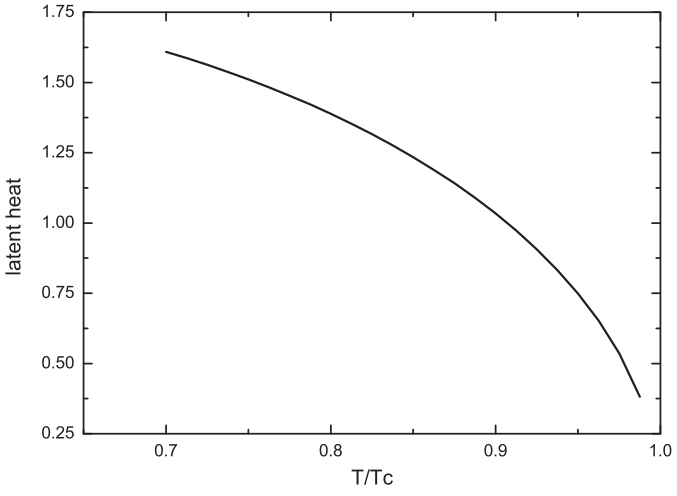

Fig. 3. Latent heat (λ) as a function of temperature for van der Waals EOS (Eq. (10)), with $a = \frac{9}{49}$, $b = \frac{2}{21}$, and $R = 1$.

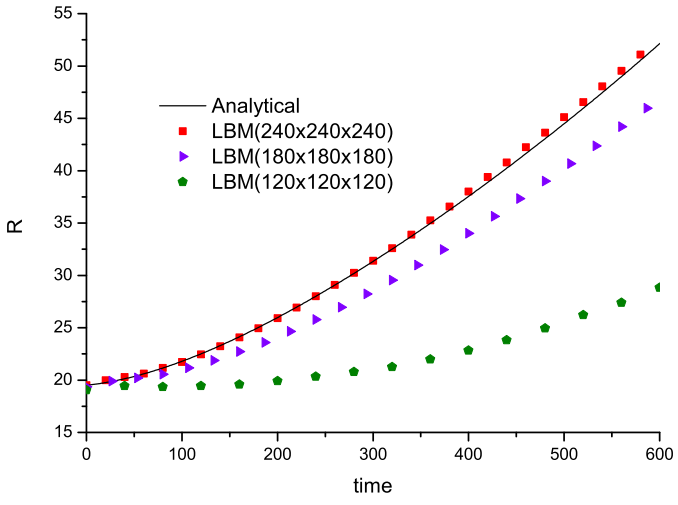

Fig. 4. Grid-independent study for bubble growth at the isothermal stage. The key parameters are $\Delta p = 0.05239\ mu/(lu\,ts^2)$, $T_0 = 0.875\ T_c$.

The isothermal growth of a single bubble in an infinite quiescent liquid can be described by Rayleigh–Plesset equation [43], i.e.,

$$\frac{p_b(t) - p_\infty(t)}{\rho_l} = \left(\frac{1}{R} - \frac{1}{r_\infty}\right)\left[2R\left(\frac{dR}{dt}\right)^2 + R^2\frac{d^2R}{dt^2}\right] - \frac{1}{2}\left(\frac{dR}{dt}\right)^2 + \frac{4\nu_l}{R}\frac{dR}{dt} + \frac{2\sigma}{\rho_l R}, \tag{24}$$

where p is pressure, ρ is density, ν is the kinematic viscosity, σ is surface tension and R is the bubble radius. The subscripts b, ∞, l represent the bubble, infinity, and liquid, respectively.

In our simulations, in order to keep the pressure constant, the improved non-equilibrium extrapolation pressure boundary condition for superheated boundary mentioned in Section 2.4 is applied on all directions. The temperature of the whole domain is set to be T_0, and it remains unchanged during the bubble growth. Suppose when temperature is T_0, at equilibrium state densities of vapor and liquid are ρ_v and ρ_l, respectively. The initial density inside the bubble ρ_{in} is set to be ρ_v, while that outside the bubble ρ_{out} is set to be slightly lower than ρ_l. That means the liquid is superheated at temperature T_0. The densities in the boundary nodes are also fixed to be $\rho_B = \rho_{out}$. Due to $\rho_{out} < \rho_l$, the pressure outside is lower than the saturated pressure at T_0. In this way the initial pressure difference across the interface is established.

First, the grid-independent study was performed. Three cases with different computational meshes were simulated. Suppose they all have dimensions of $240lu \times 240lu \times 240lu$ and total simulated time is $T = 600ts$. For computational meshes $240 \times 240 \times 240$, $180 \times 180 \times 180$, and $120 \times 120 \times 120$, the grid spacings are $\Delta x = 1\,lu$, $1.5\,lu$, and $2\,lu$, respectively. The time step sizes are $\Delta t = 1\,ts$, $1.5\,ts$, $2\,ts$, respectively. The initial bubble size is $R_i = 20\,lu$ and the other parameters are identical. e.g., $c = 1\,lu/ts$, $c_s^2 = \frac{1}{3}c^2$, $\Delta p = 0.05239\ mu/(lu\,ts^2)$ etc. It is seen from Fig. 4 that the simulation result of $240 \times 240 \times 240$ agrees well with the analytical result. The other simulation results have significant discrepancies with the analytical result but the result of $180 \times 180 \times 180$ is closer to the analytical one.

In the follows, the computational domain size is $240 \times 240 \times 240$. Fig. 5 shows radius of the bubble as a function of time for different pressure differences across the interface (Δp) at $T_0 = 0.875T_c$. The key parameters are listed in Table 1. The

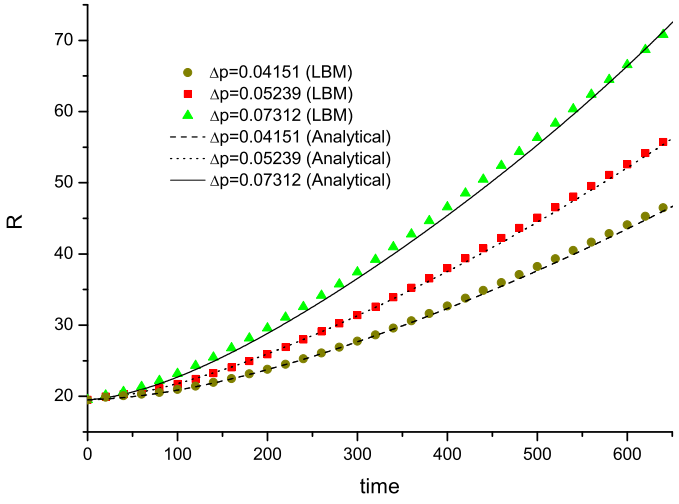

Fig. 5. Radius of the bubble as a function of time for different pressure differences across the interface Δp at a constant temperature $T_0 = 0.875\ T_c$.

Table 1
The key parameters in the cases presented in Fig. 5. The inside and outside pressures can be calculated from the EOS with ρ_{in} and ρ_{out}, respectively.

Case	$\frac{T}{T_c}$	τ	ρ_{in}	$\rho_{out}(\rho_B)$	Δp
1	0.875	1.0	1.420	6.040	0.04151
2	0.875	1.0	1.420	6.020	0.05239
3	0.875	1.0	1.420	5.980	0.07312

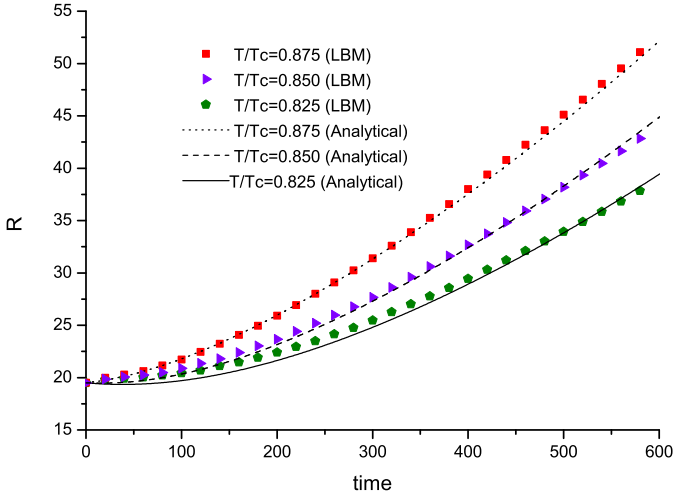

Fig. 6. Radius of the bubble as a function of time at different temperature with $\Delta p = 0.05239\, mu/(lu\, ts^2)$.

initial bubble radius is $R_i = 19.5\, lu$. In the figure, the analytical solutions are also drawn for comparison. The analytical solutions are obtained through solving Eq. (24) by the fourth-order Runge–Kutta method. Due to limitation of our computational domain, r_∞ in the solution is chosen to be 120 lu, which is the half size of each dimension. It is seen from the figure that the LBM results agree well with the theoretical solutions.

The isothermal growth stage at different temperatures were also simulated. Fig. 6 shows the radius of the bubble as a function of time at different temperatures with $\Delta p = 0.05239\, mu/(lu\, ts^2)$. The key parameters are listed in Table 2. From the figure it is seen that the LBM results also agree well with the theoretical solutions. In addition, we can see that when Δp is fixed, the bubble growth rate can be enhanced by the temperature of the liquid. The higher the temperature is, the faster the bubble grows.

Table 2
The key parameters in the cases presented in Fig. 6.

Case	$\frac{T}{T_c}$	τ	ρ_{in}	$\rho_{out}(\rho_B)$	Δp
A	0.875	1.0	1.420	6.020	0.05239
B	0.850	1.0	1.290	6.295	0.05239
C	0.825	1.0	1.150	6.534	0.05239

4.2. Isobaric growth stage

After the short isothermal growth stage ends, the bubble's volume increases to a certain extent. Both the pressure and temperature inside the bubble decrease. The inertial effect is diminished. Then the bubble growth enters the second stage, i.e., isobaric growth stage. In this stage, the bubble growth mainly depends on the heat transfer of the superheated liquid. So this stage is also called the heat-controlled stage.

Based on the D^2 law of droplet evaporation [44], the three-dimensional spherical bubble growth at the isobaric stage in infinite quiescent liquid can be described by

$$R^2\left(1-\frac{2R}{3r_\infty}\right) = R_i^2\left(1-\frac{2R_i}{3r_\infty}\right) + \frac{2\rho_s\alpha_s}{\rho_v} ln(1+B)t, \tag{25}$$

where R is the bubble radius, R_i is the initial bubble radius, α_s is the thermal diffusivity at the interface. The subscript s denotes the bubble interface. The coefficient $B = c_p(T_\infty - T_v)/\lambda$, where c_p is the specific heat at constant pressure.

In the LBM simulation, the computational domain size is $192 \times 192 \times 192$ and the origin of coordinates (0,0,0) is located at the center of the computational domain. It is reasonable to set $r_\infty = 96\, lu$. Before the temperature boundary condition is imposed, the bubble and liquid densities are allowed to reach an equilibrium state at the temperature of the saturated liquid, i.e., T_0. Then the Dirichlet boundary condition with $T_1 = T_0 + \Delta T$ is set on all directions. The velocity and inter-particle force at boundary nodes are extrapolated from the neighbouring fluid nodes. It is noted that for an edge point, e.g., (x_1, y_1, z_1), where $x_1 = 96\, lu$, $y_1 = 96\, lu$, and $z_1 \neq 1\, lu, 192\, lu$, the velocity and inter-particle force are extrapolated from point (x_2, y_2, z_1), where $x_2 = 95\, lu$, $y_2 = 95\, lu$. For a corner point, e.g., (96,96,96), its velocity and inter-particle force are extrapolated from the point (95,95,95). For pressure, the non-equilibrium extrapolation boundary condition [41] described in Section 2.4 is applied to ensure the pressure is equal the saturation pressure at the corresponding temperature T_0. If not speci-

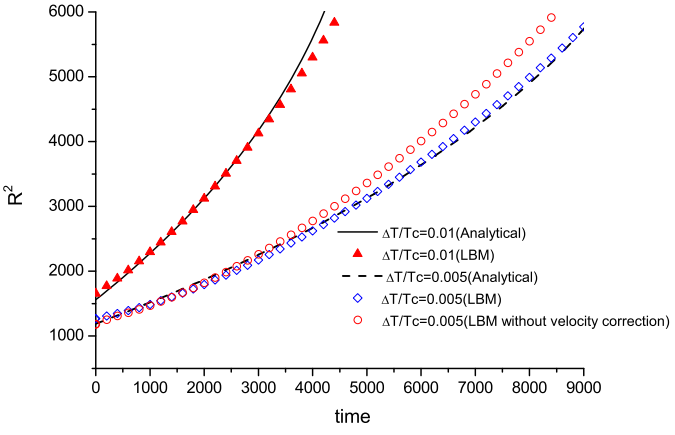

Fig. 7. Isobaric growth curves with different superheat at $\frac{T}{T_c} = 0.875$.

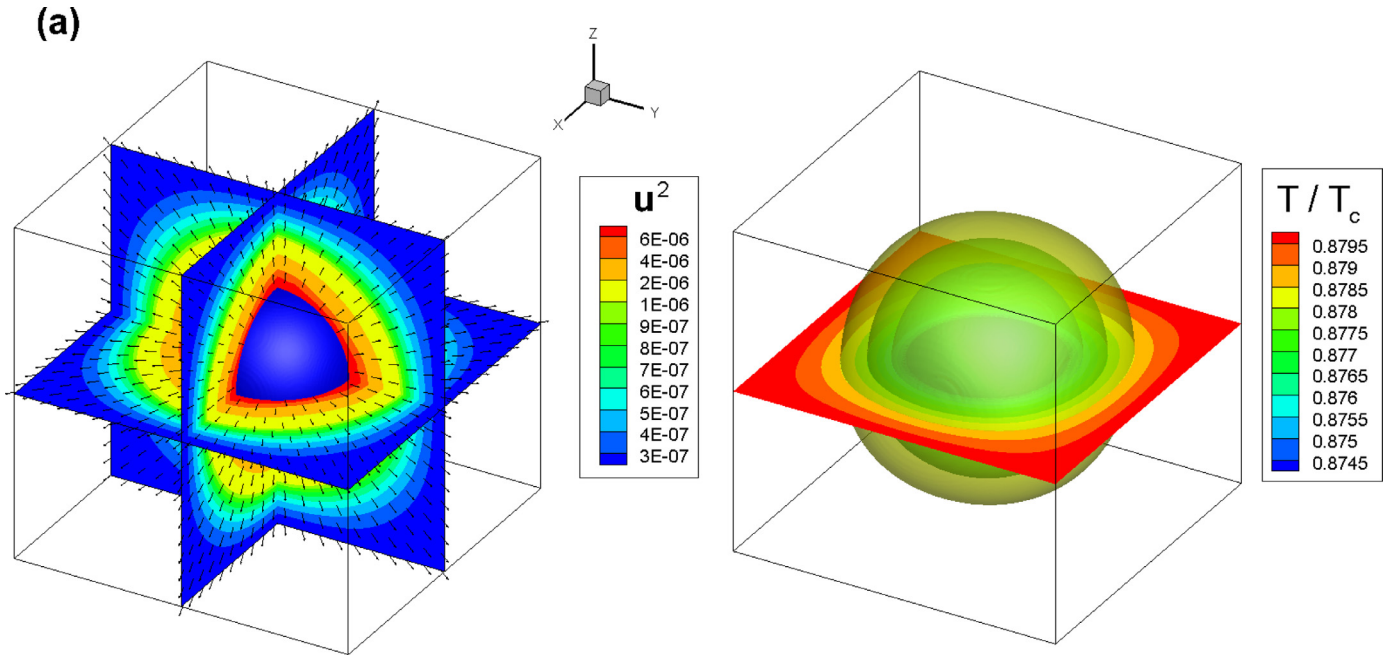

Fig. 8. (a) Velocity field for the case $\Delta T/T_c = 0.005$ at $t = 1800\,ts$. The vectors in planes $x = 0$, $y = 0$, and $z = 0$ represent the velocity directions at the points (vector length is uniform). The contours for the velocity squared are shown in the planes. The central blue sphere represents the bubble. (b) The temperature field for the case $\Delta T/T_c = 0.005$ at $t = 1800\,ts$. Isosurfaces with $T/T_c = 0.876,\ 0.8775,\ 0.8785$ are presented. (For interpretation of the references to colour in this figure legend, the reader is referred to the web version of this article.)

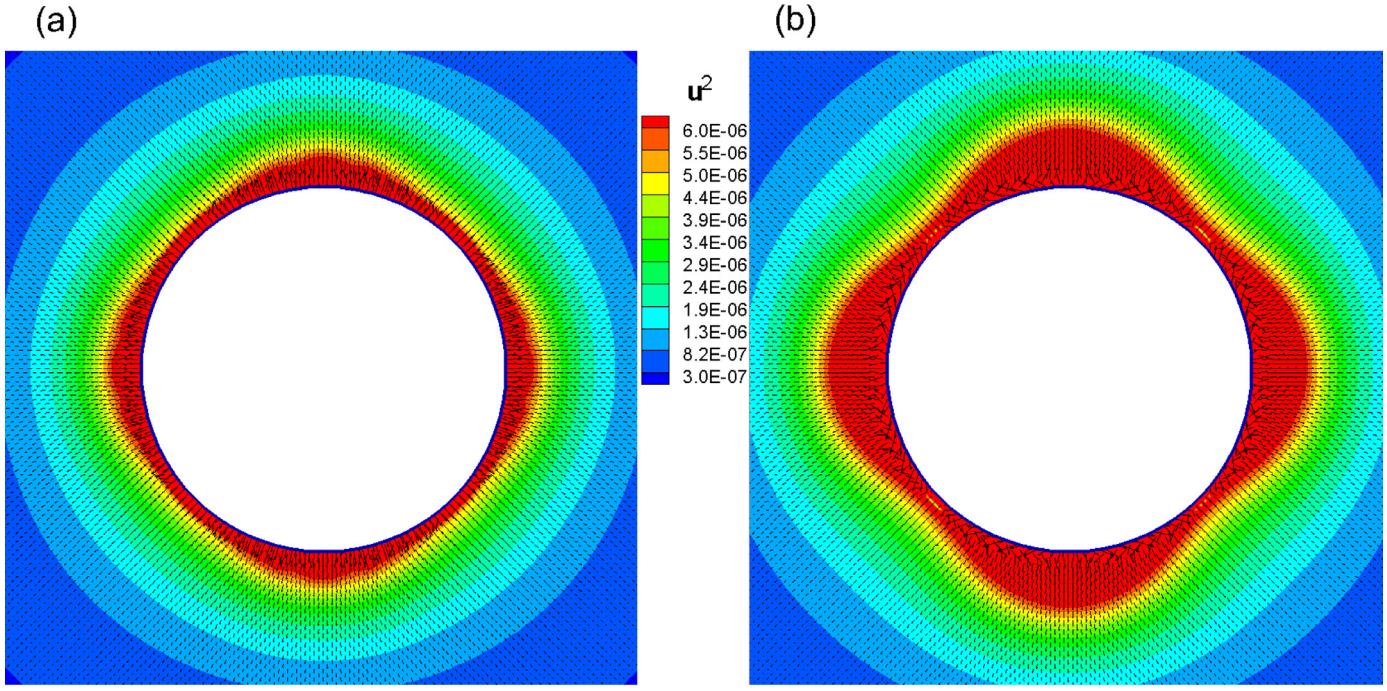

Fig. 9. A zoom-in view of the velocity vectors in the vicinity of the bubble in the $z = 0$ plane with the contours for $\mathbf{u}^2$ at $t = 1800\,ts$. (a) Corrected velocity field, (b) original flow field with spurious currents.

fied, in our LBM simulations, the level-set scheme is incorporated to correct the spurious currents in the vicinity of the interface.

Fig. 7 shows the radius squared of the bubble as a function of time when the boundary superheat ΔT is fixed to be $\Delta T = 0.005\ T_c$ and $0.01T_c$, respectively. The initial bubble radii are $R_i = 34.5\,lu$ and $R_i = 39.5\,lu$, respectively for the above two superheats. The key parameters in the simulations are $T = 0.875T_c$, $c_p = 30$, $\alpha_s = 0.5$ and $\tau = 1.0$. The initial densities of vapor and liquid are set to be the equilibrium densities at T_0, e.g., $\rho_{in} = 1.42\,mu/lu^3$ and $\rho_{out} = 6.094\,mu/lu^3$ for $T_0 = 0.875T_c$. The liquid density at boundary is $\rho_B = 6.0230\,mu/lu^3$ for $\Delta T = 0.005T_c$ and $\rho_B = 5.9476\,mu/lu^3$ for $\Delta T = 0.01T_c$. It is seen from Fig. 7, the LBM results are consistent with the analytical solutions given by Eq. (25). It is found that increasing the superheat at the boundaries can significantly accelerate the bubble growth. The LBM result for $\Delta T = 0.005T_c$ without velocity correction is also presented in Fig. 7 for comparison. We can see the result of the simulation without velocity correction has significant discrepancy with the

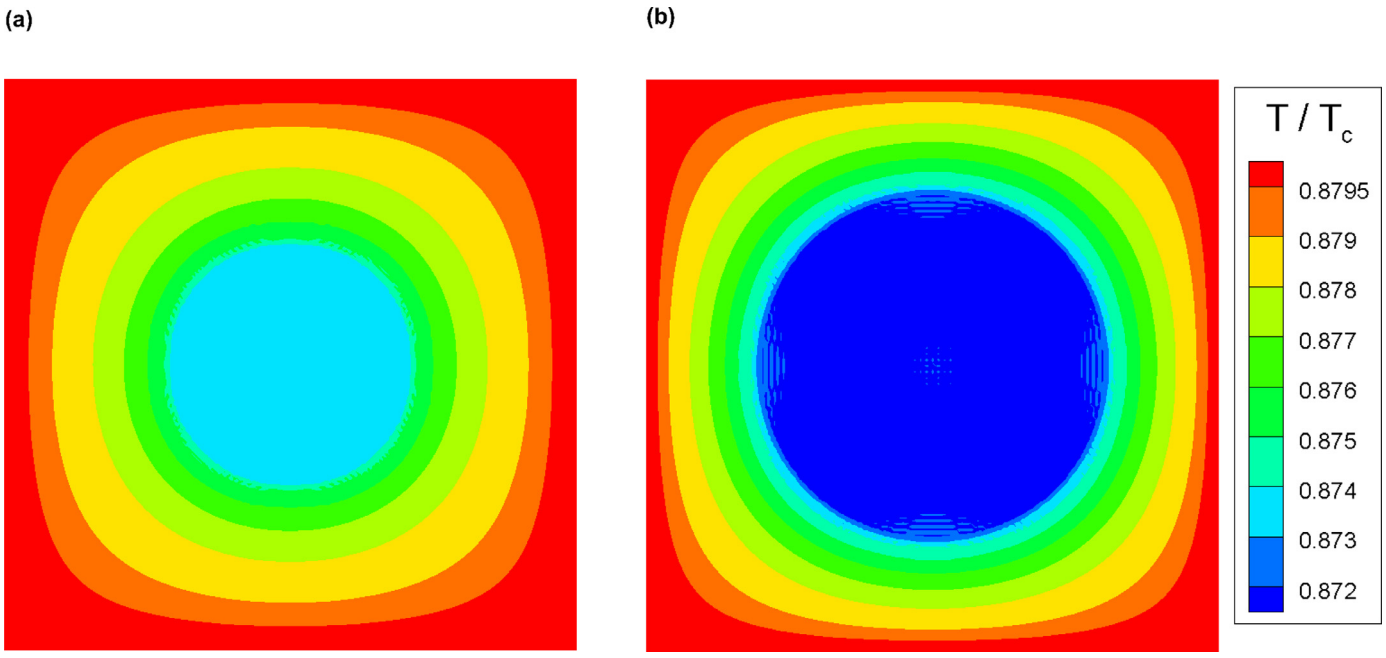

Fig. 10. The temperature contours on slice $z = 0$ at (a) $t = 1800\,ts$ and (b) $t = 5800\,ts$.

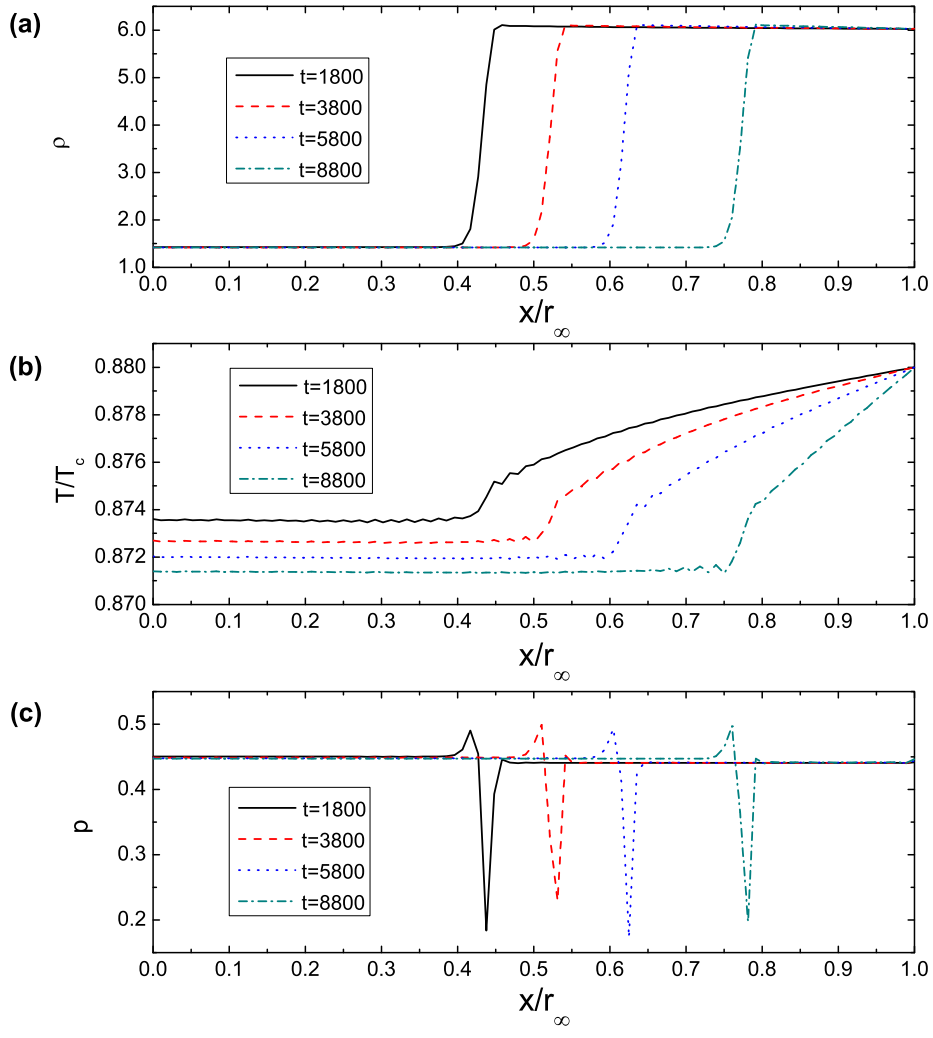

Fig. 11. The macro variables (a) density, (b) temperature and (c) pressure as functions of the distance from the origin of coordinates (0,0,0) on the $z = 0$ plane.

analytical solution. Hence, the velocity correction improves simulation accuracy for the bubble growth.

Fig. 8(a) shows the velocity field for the case $\Delta T/T_c = 0.005$ at $t = 1800\,ts$. It is seen that during the bubble growth, the bubble squeezes the surrounding liquid, which pushes the liquid to flow outwardly. Due to the correction of spurious currents, the isosurfaces for the velocity squared are close to spherical. The velocity vector at any point on the sphere is perpendicular to the local surface. Fig. 9(a) shows the velocity field with velocity correction in the vicinity of the interface in the $z = 0$ plane. The contours for the velocity squared in the vicinity of the bubble are also close to circular. However, if the spurious currents are presented, the contours for $\mathbf{u}^2$ in the vicinity of the bubble is not circular (see Fig. 9(b)). From the comparison between Fig. 9(a) and (b), it is seen that the velocity correction does improve the representation of interfacial dynamics. On the other hand, it is also seen from Fig. 8(a), the isosurfaces for $\mathbf{u}^2$ close to the boundary of the finite computational domain may be not so spherical due to the effect of boundary.

Fig. 8(b) shows the temperature field at $t = 1800\,ts$ with $\Delta T = 0.005\ T_c$. It is seen that the isosurfaces for the temperature are also spherical. The temperature contours on slice $z = 0$ at (a) $t = 1800\,ts$ and (b) $t = 5800\,ts$ are shown in Fig. 10. It is seen that as time evolves the temperature of the vapor inside the bubble decreases a little bit.

Fig. 11(a), (b), and (c) show the density, temperature and pressure distribution at different time during bubble growth with $\Delta T = 0.005\ T_c$. It is seen that the vapor-liquid interface moves as time evolves, i.e., bubble grows.

From Fig. 11 (c), it is seen that during this growth stage, the pressures inside and outside of the bubble are almost identical because the pressure due to surface tension is negligible. The bubble growth is attributed to the heat transfer from the liquid to the vapor-liquid interface, which make the liquid film evaporate. It is seen that at a specific time, the temperature inside the bubble remains constant, e.g., the temperature inside the bubble is $\frac{T}{T_c} \approx 0.874$ at $t = 1800\,ts$. As the bubble grows, the temperature in the bubble may slightly decrease, as shown in Figs. 10 or 11 (b). The decrease may be due to the heat absorbtion when liquid film evaporates. When the liquid film close to the interface evaporates, it absorbs not only the heat from the liquid but also that inside the bubble. It is noted that the temperature distribution from the interface to the boundary (e.g., approximately $\frac{x}{r} \in (0.4, 1)$ at $t = 1800\,ts$) represents the heat transfer outside the bubble (inside the liquid region) instead of that in the thermal boundary layer at the interface.

In the follows, the mass conservation issue during the simulation at the isobaric growth stage is also investigated. Due to evaporation, a very small portion of liquid changes into vapor, and therefore the mass of vapor increases. The mass of liquid in the fixed computational domain decreases mainly because the growth of bubble pushes the liquid away from the domain. Total mass (m_{total}) in our study consists of vapor mass (m_v), liquid mass inside the computational domain (m_l), and liquid left the domain (m_{out}). They are functions of time, and can be calculated through

$$m_v(t) = \sum_{\mathbf{x}\in\Omega_v} \rho(\mathbf{x})\Delta V, \tag{26}$$

$$m_l(t) = \sum_{\mathbf{x}\in\Omega_l} \rho(\mathbf{x})\Delta V, \tag{27}$$

$$m_{out}(t) = \sum_{t}\sum_{\mathbf{x}\in\Gamma} \rho(\mathbf{x})(\mathbf{u}(\mathbf{x})\cdot\mathbf{n}')\Delta t\Delta S, \tag{28}$$

$$m_{total}(t) = m_v + m_l + m_{out}, \tag{29}$$

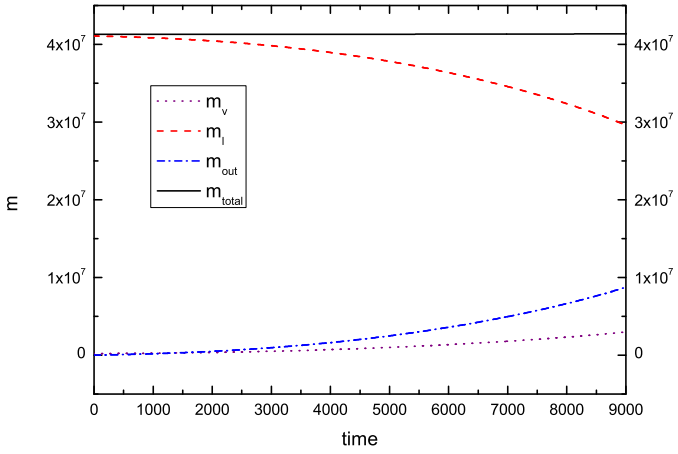

Fig. 12. Vapor mass (m_v), liquid mass inside the computational domain (m_l), liquid mass left the domain (m_{out}), and total mass (m_{total}) as functions of time.

where $\Delta t = 1\,ts$, $\Delta V = \Delta x\Delta y\Delta z$, $\Delta x = \Delta y = \Delta z = 1\,lu$. Ω_v and Ω_l denote regions occupied by the vapor and liquid, respectively. In the regions, we have $\rho(\mathbf{x}) < \rho_s$ and $\rho(\mathbf{x}) \geq \rho_s$, respectively. Here Γ represents the outside boundary of the whole computational domain $\Omega = \Omega_v \cup \Omega_l$. The interface is supposed to be located at $\rho_s = \frac{1}{2}(\rho_l + \rho_v)$. $\mathbf{n}'$ is the unit vector normal to the boundary Γ and $(\mathbf{u}\cdot\mathbf{n}')$ denotes the flow velocity normal to the boundary. $\Delta S = \Delta x\Delta y$, or $\Delta y\Delta z$, or $\Delta z\Delta x$. It represents a finite surface normal to the local vector $\mathbf{n}'$. It is seen from Fig. 12 that at any time, the solid line is horizontal and the total mass m_{total} is a constant. Hence, in the simulation, the mass conservation is well satisfied.

5. Conclusion

The two growth stages for a single bubble, i.e., the isothermal and isobaric stages in a finite domain of quiescent liquid are studied using a hybrid thermal lattice Boltzmann model. An improved non-equilibrium extrapolation pressure boundary condition is adopted for the superheated boundary. Unfavorable spurious currents in the vicinity of the interface are successfully corrected by a level-set scheme. The bubble growth rate obtained from the LB simulations are consistent with the analytical solutions. It shows that the present scheme is able to simulate relevant thermal bubble dynamics quantitatively.

Acknowledgment

Huang is supported by National Natural Science Foundation of China (Grant No. 11472269). X.Y.L is supported by National Natural Science Foundation of China (NSFC) grant no. 11621202.

Appendix A. Derivation of Rayleigh–Plesset equation

The derivation of Rayleigh–Plesset equation, i.e. Eq. (24) is given by Brennen [43]. In the liquid, the conservation of mass requires that

$$u(r,t) = \frac{F(t)}{r^2}, \tag{A.1}$$

where $F(t)$ is related to the bubble radius $R(t)$ by a kinematic boundary condition at the bubble surface and $u(r, t)$ is the radial velocity in a spherical coordinate system. we also have $u(R,t) = dR/dt$, therefore

$$F(t) = R^2\frac{dR}{dt}. \tag{A.2}$$

Assuming a Newtonian liquid and abandoning the viscous terms, the Navier–Stokes equation for motion in the r direction,

$$-\frac{1}{\rho_l}\frac{\partial p}{\partial r} = \frac{\partial u}{\partial t} + u\frac{\partial u}{\partial r}. \tag{A.3}$$

Substituting the Eq. (A.1) into Eq. (A.3), we obtain

$$-\frac{1}{\rho_l}\frac{\partial p}{\partial r} = \frac{1}{r^2}\frac{dF}{dt} - \frac{2F^2}{r^5}. \tag{A.4}$$

Integrating Eq. (A.4) from R to r_∞, we have

$$\frac{p - p_\infty}{\rho_l} = \left(\frac{1}{R} - \frac{1}{r_\infty}\right)\frac{dF}{dt} - \frac{1}{2}\frac{F^2}{R^4}. \tag{A.5}$$

A pressure boundary condition at the bubble surface is written as

$$p_b - (p)_{r=R} - \frac{4\mu_l}{R}\frac{dR}{dt} - \frac{2\sigma}{R} = 0, \tag{A.6}$$

where μ_l is the dynamic viscosity of liquid and the subscript b denotes the bubble. Substituting Eqs. (A.2) and (A.6) into (A.5), we have the Rayleigh–Plesset equation

$$\frac{p_b(t) - p_\infty(t)}{\rho_l} = \left(\frac{1}{R} - \frac{1}{r_\infty}\right)\left[2R\left(\frac{dR}{dt}\right)^2 + R^2\frac{d^2R}{dt^2}\right] - \frac{1}{2}\left(\frac{dR}{dt}\right)^2 + \frac{4\nu_l}{R}\frac{dR}{dt} + \frac{2\sigma}{\rho_l R}. \tag{A.7}$$

For the bubble growth at the isothermal stage (an inertia-controlled stage), the nondimensional pressure difference $\Delta p^* = \frac{p_b - p_\infty}{\rho_l\left(\frac{\Delta x}{\Delta t}\right)^2}$ controls the bubble growth.

Appendix B. Derivation of equation of bubble isobaric growth in superheat liquid

The single-component equation of heat transfer in a spherical coordinate is given by

$$r^2\rho c_p u\frac{dT}{dr} = \frac{d}{dr}\left(r^2\kappa\frac{dT}{dr}\right). \tag{B.1}$$

From the integrated continuity equation, we get

$$r^2\rho u = r_s^2\rho_s u_s, \tag{B.2}$$

where subscript s denotes the bubble interface. Therefore, the Eq. (B.1) can be rewritten as

$$r_s^2\rho_s u_s c_p\frac{dT}{dr} = \frac{d}{dr}\left(r^2\kappa\frac{dT}{dr}\right). \tag{B.3}$$

The boundary condition of energy balance at the bubble interface is given by

$$\kappa\left(\frac{dT}{dr}\right)_s = \rho_s u_s\lambda. \tag{B.4}$$

Using Eq. (B.4), we integrate Eq. (B.3), and have

$$r_s^2\rho_s u_s c_p\left(T - T_s + \frac{\lambda}{c_p}\right) = r^2\kappa\frac{dT}{dr}. \tag{B.5}$$

After separating the variables and integrating Eq. (B.5) with the boundary condition that $T \to T_\infty$ as $r \to \infty$, we have

$$\frac{r_s^2\rho_s u_s c_p}{\kappa}\left(\frac{1}{r} - \frac{1}{r_\infty}\right) = \ln\left(\frac{T_\infty - T_s + \lambda/c_p}{T - T_s + \lambda/c_p}\right). \tag{B.6}$$

Considering $r = r_s$ at the surface, we have

$$r_s^2 u_s\left(\frac{1}{r_s} - \frac{1}{r_\infty}\right) = \alpha_s\ln\left[1 + \frac{c_p(T_\infty - T_s)}{\lambda}\right] \equiv \alpha_s\ln[1 + B], \tag{B.7}$$

where $\alpha_s = \frac{\kappa}{\rho_s c_p}$ and $B = \frac{c_p(T_\infty - T_s)}{\lambda}$. The mass continuity at the bubble surface is given by

$$\rho_v\frac{dr_s}{dt} = \rho_s u_s. \tag{B.8}$$

Using Eq. (B.8), we have

$$r_s^2\left(\frac{1}{r_s} - \frac{1}{r_\infty}\right)\frac{dr_s}{dt} = \frac{\rho_s\alpha_s}{\rho_v}\ln(1 + B). \tag{B.9}$$

Finally, separating the variables and integrating Eq. (B.9) for with an initial bubble radius R_0, we get the equation of bubble isobaric growth in superheat liquid, which is written as

$$R^2\left(1 - \frac{2R}{3r_\infty}\right) = R_i^2\left(1 - \frac{2R_i}{3r_\infty}\right) + \frac{2\rho_s\alpha_s}{\rho_v}ln(1 + B)t. \tag{B.10}$$

For the bubble growth at the isobaric stage, the Jakob number $Ja = \frac{\rho_l c_p(T_\infty - T_s)}{\rho_g\lambda}$ controls the growth.

References

[1] Tong LS, Tang YS. Boiling heat transfer and two-phase flow. CRC press; 1997.
[2] Lee HC, Do Oh B, Bae SW, Kim MH. Single bubble growth in saturated pool boiling on a constant wall temperature surface. Int J Multiphase Flow 2003;29(12):1857–74.
[3] Mukherjee A, Dhir V. Study of lateral merger of vapor bubbles during nucleate pool boiling. Trans ASME, J Heat Transfer 2004;126(6):1023–39.
[4] Forster H, Zuber N. Growth of a vapor bubble in a superheated liquid. J Appl Phys 1954;25(4):474–8.
[5] Chesters A. An analytical solution for the profile and volume of a small drop or bubble symmetrical about a vertical axis. J Fluid Mech 1977;81(04):609–24.
[6] Prosperetti A, Plesset MS. Vapour-bubble growth in a superheated liquid. J Fluid Mech 1978;85(02):349–68.
[7] Son G, Dhir V. Numerical simulation of saturated film boiling on a horizontal surface. Trans ASME, J Heat Transfer 1997;119:525–33.
[8] Welch SW, Wilson J. A volume of fluid based method for fluid flows with phase change. J Comput Phys 2000;160(2):662–82.
[9] Ling K, Li Z-Y, Tao W-Q. A direct numerical simulation for nucleate boiling by the voset method. Numer Heat Transfer, Part A 2014;65(10):949–71.
[10] Yoon HY, Koshizuka S, Oka Y. Direct calculation of bubble growth, departure, and rise in nucleate pool boiling. Int J Multiphase Flow 2001;27(2):277–98.
[11] Házi G, Markus A. On the bubble departure diameter and release frequency based on numerical simulation results. Int J Heat Mass Transf 2009;52(5):1472–80.
[12] Shan X, Doolen G. Multicomponent lattice-Boltzmann model with interparticle interaction. J Stat Phys 1995;81(1):379–93.
[13] Benzi R, Biferale L, Sbragaglia M, Succi S, Toschi F. Mesoscopic modeling of a two-phase flow in the presence of boundaries: the contact angle. Phys RevE 2006;74(2):021509.
[14] Inamuro T, Ogata T, Tajima S, Konishi N. A lattice Boltzmann method for incompressible two-phase flows with large density differences. J Comput Phys 2004;198(2):628–44.
[15] Cheng M, Hua J, Lou J. Simulation of bubble–bubble interaction using a lattice Boltzmann method. Comput Fluids 2010;39(2):260–70.
[16] Amaya-Bower L, Lee T. Single bubble rising dynamics for moderate Reynolds number using lattice Boltzmann method. Comput Fluids 2010;39(7):1191–207.
[17] Gunstensen AK, Rothman DH, Zaleski S, Zanetti G. Lattice Boltzmann model of immiscible fluids. Phys Rev A 1991;43(8):4320.
[18] Rothman DH, Keller JM. Immiscible cellular-automaton fluids. J Stat Phys 1988;52(3):1119–27.
[19] Shan X, Chen H. Lattice Boltzmann model for simulating flows with multiple phases and components. Phys Revi E 1993;47(3):1815.
[20] Swift MR, Orlandini E, Osborn WR, Yeomans JM. Lattice Boltzmann simulations of liquid-gas and binary fluid systems. Phys Rev E 1996;54(5):5041–52.
[21] He X, Chen S, Zhang R. A lattice Boltzmann scheme for incompressible multiphase flow and its application in simulation of rayleigh–taylor instability. J Comput Phys 1999;152(2):642–63.
[22] Safari H, Rahimian MH, Krafczyk M. Consistent simulation of droplet evaporation based on the phase-field multiphase lattice Boltzmann method. Phys Rev E 2014;90(3):033305.
[23] Ryu S, Ko S. Direct numerical simulation of nucleate pool boiling using a two-dimensional lattice Boltzmann method. Nucl Eng Des 2012;248:248–62.
[24] Lee T, Liu L. Lattice boltzmann simulations of micron-scale drop impact on dry surfaces. J Comput Phys 2010;229(20):8045–63.
[25] Li Q, Kang Q, Francois MM, He Y, Luo K. Lattice Boltzmann modeling of boiling heat transfer: the boiling curve and the effects of wettability. Int J Heat Mass Transf 2015;85:787–96.
[26] Markus A, Házi G. Simulation of evaporation by an extension of the pseudopotential lattice Boltzmann method: a quantitative analysis. Physical Review E 2011;83(4).
[27] Biferale L, Perlekar P, Sbragaglia M, Toschi F. Convection in multiphase fluid flows using lattice Boltzmann methods. Phys Rev Lett 2012;108(10):104502.

[28] Gong S, Cheng P. A lattice Boltzmann method for simulation of liquid–vapor phase-change heat transfer. Int J Heat Mass Transf 2012;55(17):4923–7.
[29] Gong S, Cheng P. Lattice Boltzmann simulation of periodic bubble nucleation, growth and departure from a heated surface in pool boiling. Int J Heat Mass Transf 2013;64:122–32.
[30] Fang W-Z, Chen L, Kang Q-J, Tao W-Q. Lattice Boltzmann modeling of pool boiling with large liquid-gas density ratio. Int J Therm Sci 2017;114:172–83.
[31] Palmer BJ, Rector DR. Lattice-Boltzmann algorithm for simulating thermal two-phase flow. Phys Rev E 2000;61(5):5295.
[32] Albernaz DL, Amberg G, Do-Quang M. Simulation of a suspended droplet under evaporation with marangoni effects. Int J Heat Mass Transf 2016;97:853–860.
[33] Chen X-P, Zhong C-W, Yuan X-L. Lattice Boltzmann simulation of cavitating bubble growth with large density ratio. Comput Math Appl 2011;61(12):3577–84.
[34] Zheng HW, Shu C, Chew YT. A lattice Boltzmann model for multiphase flows with large density ratio. J Comput Phys 2006;218(1):353–71.
[35] Dong Z, Li W, Song Y. A numerical investigation of bubble growth on and departure from a superheated wall by lattice Boltzmann method. Int J Heat Mass Transf 2010;53(21):4908–16.
[36] Martys NS, Chen H. Simulation of multicomponent fluids in complex three--dimensional geometries by the lattice Boltzmann method. Phys Rev E 1996;53(1):743.
[37] Shan X, Chen H. Simulation of nonideal gases and liquid-gas phase transitions by the lattice Boltzmann equation. Phys Rev E 1994;49(4):2941.
[38] Yuan P, Schaefer L. Equations of state in a lattice Boltzmann model. Phys Fluids 2006;18(4):042101.
[39] Mcclure JE, Berrill M, Gray W, Miller C. Tracking interface and common curve dynamics for two-fluid flow in porous media. J Fluid Mech 2016;796:211–32.
[40] Sbragaglia M, Benzi R, Biferale L, Succi S, Sugiyama K, Toschi F. Generalized lattice Boltzmann method with multirange pseudopotential. Phys Revi E 2007;75(2):026702.
[41] Guo ZL, Zheng CG, Shi BC. Non-equilibrium extrapolation method for velocity and pressure boundary conditions in the lattice Boltzmann method. Chin Phys 2002;11(4):366–74.
[42] Huang H, Sukop M, Lu X. Multiphase lattice Boltzmann methods: theory and application. John Wiley & Sons; 2015.
[43] Brennen CE. Cavitation and bubble dynamics. Cambridge University Press; 2013.
[44] Kuo KK. Principles of combustion. John Wiley & Sons, Inc; 1986.